Journal of Materials Chemistry A

Accepted Manuscript

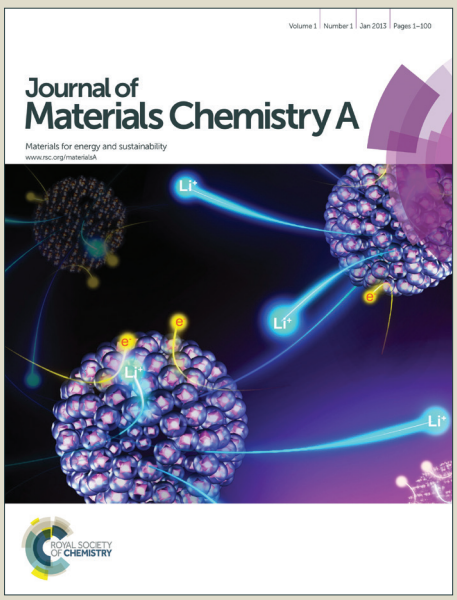

ROYAL SOCIETY OF CHEMISTRY

www.rsc.org/materialsA

Journal of Materials Chemistry A RSCPublishing

COMMUNICATION

Carambola-shaped $LiFePO_4$/C nanocomposites: directing synthesis and enhanced Li storage properties †

Cite this: DOI: 10.1039/x0xx00000x

Xueliang Li,*[a] Hongchang Jin,[a] Shuai Liu,[a] Sen Xin,[a] Yu Meng,[a] and Jiejie Chen[b]

Received ooth,
Accepted ooth

DOI: 10.1039/x0xx00000x

www.rsc.org/

Carbon-coated carambola-like $LiFePO_4$, which consists of $LiFePO_4$ thin layers with selectively exposed (020) plane was synthesized by a new method via oriented growth with cholesteric benzoate as structure-directing agent. The composite exhibits stable and extremely fast kinetics upon Li storage.

Lithium-ion batteries (LIBs) have been regarded as one of the most promising solutions for emerging transportation applications including electric vehicles (EVs) and hybrid electric vehicles (HEVs).[1-4] To meet the demands on vehicle endurance and service life, batteries are often required to have high theoretical capacities and long life span. In either case, LIBs based on olivine $LiFePO_4$ (LFP) cathode could yield satisfactory results due to a large capacity and favorable cyclability of LFP,[5-6] with its low price and environmental friendliness adding the cost effectiveness of the battery.[7-10] However, with a raising demand on the power density of the battery, the use of LFP-based LIBs is hindered by their poor electrochemical reaction kinetics due to intrisincally low Li-ion diffusivity (~1.8×10^{-14} cm^2 s^{-1}) and electronic conductivity of LFP.[7, 11-14]

The combination with conductive carbon has been proved effectively in solving the insulating problem of LFP,[15-19] yet has a limited effect in improving its Li^+ diffusivity. Reduction of particle size is a common way to enhance the Li^+ mobility due to its role in shortening the Li^+ migration pathway,[20, 21] however, it is not fully applicable to LFP. The reason lies in the crystal structure of olivine LFP, which allows a preferential Li migration along the $[010]_{Pnma}$ channel.[22] Therefore, only decreasing the length of the [010] pathway can effectively enhance the Li^+ mobility of LFP.

Based on this concept, LFP with selectively exposed (020) plane and short [010] channel is especially promising, yet its synthesis is still challenging. In this paper, a novel directing synthesis procedure has been designed for LFP, which employs a cholesteric liquid crystal, cholesteryl benzoate (CB), as the structuredirecting agent to achieve the oriented growth of LFP along the designated direction. A carambola-like LFP (c-LFP) is prepared, which consists of LFP thin layers with significantly shortened [010] channel of ~15 nm and selectively exposed (020) plane. The unique structure greatly promotes the Li^+ diffusion along the preferential direction for Li storage, bringing an unprecedented Li^+ diffusion coefficient of 8.31×10^{-9} cm^2 s^{-1}, which is five orders of magnitude large than that with the bulk LFP. On the other hand, we have successfully coated a highly-conductive unltrathin carbon layer with controllable thickness (~1.5 nm) onto the surface of $LiFePO_4$ sheets, enabling fast electron transportation along the two-dimensional sheet. With the structural advantages of both components, a hierarchically mixed conductive network is formed, which triggers fast electrode kinetics by enabling bidirectional efficient transmissions of both Li^+ and e^-. The composite exhibits stable and extremely fast electrochemistry upon Li storage by delivering almost a theoretical capacity (167 mA h g^{-1}) at 0.1 C and ~50% of the theoretical capacity (82 mA h g^{-1}) at a high rate of 20 C, and keeps stable cycling performances at different rates. All these promise its use in constructing batteries with stable electrochemistry and high energy output to benefit the emerging EV industry.

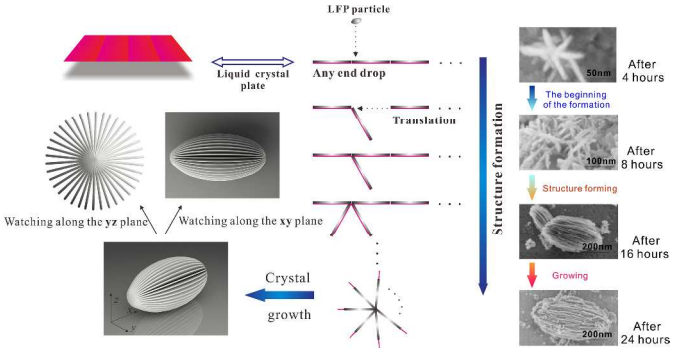

Figure 1. Schematic representation of the fabrication process of c-LFP nanocrystals and SEM images of c-LFP in the different stage of formation process.

The preparation of carambola-shaped $LiFePO_4$ is shown in Figure 1. Liquid crystals (LC) are intermediate states between crystals and isotropic liquids and thus have intermediate physical properties between them.[23] The molecular planes of cholesteryl benzoate are perpendicular to the helical axis, presenting a preferred average orientation.[24] As cholesteric liquid crystals, CB has spontaneous periodic structures consisting of nematic layers, and these

characteristics have been used to synthesize LFP nanocrystals with target structure. In the process of the reaction, the liquid crystal nematic layers are suspended in the ethylene glycol under magnetic stirring. And the LFP layers fall on the surface of nematic layers. Then the LC molecules guide these LFP layers to form carambola-shaped structure, meanwhile, these LFP are growing. In this process, nano-size LFP thin layers fabricated the c-LFP through the miraculous effect of liquid crystal. Compared with the n-LFP, c-LFP has smaller particle size and thinner layers. The SEM images in Figure 1 show the formation process of c-LFP in the different stages. There are two stages in this process, which are structure forming procedure and particle growing procedure. And the mechanism confirm to the formation process generally.

The structure of the samples was characterized by field emission scanning electron microscopy (FESEM), transmission electron microscopy (TEM) and high resolution transmission electron microscopy (HRTEM). Figure 2a displays an FESEM image of the LFP particles synthesized by solvothermal at 160 °C for 8 hours. These petal shaped LFP show a quite uniform distribution of particle size with average diameter of ~500 nm, length of ~1 μm. From the higher magnified SEM images (Fig. 2b), it can be clearly observed that these similar in size of the LFP petals are stack together without rules. Figure 2c shows the typical sample synthesized by mixing LC with a very uniform, carambola-like architecture ~400 nm in diameter and ~700 nm in length. The detailed morphology of the carambola-like nanostructure is shown in the Figure 2d, which reveals the entire lamellar surface. Interestingly, each nanopetal connected to each other through the center to form hierarchically carambola structures, which can be vividly demonstrated by the SEM images of a sphere fringe (Figs. 2d).

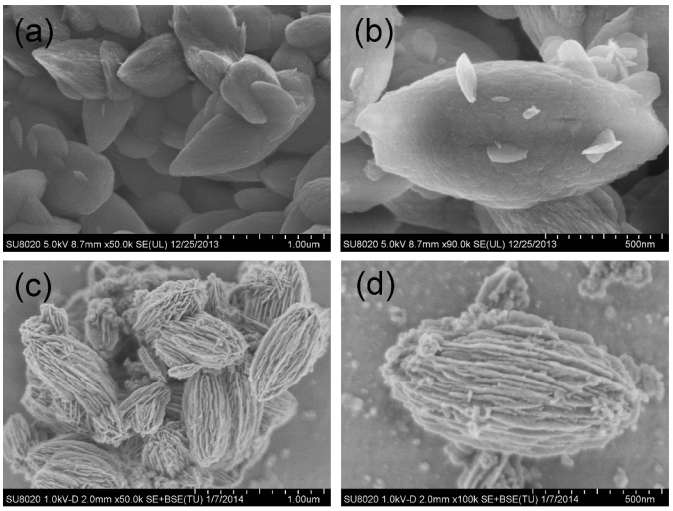

Figure 2. FESEM images (a) and (b) of n-LFP, (c) and (d) of c-LFP.

X-ray diffraction (XRD) patterns of the as-synthesized LFP and carbon coated LFP materials are shown in Figure S1 (see experimental details in the ESI†). All diffraction peaks agree well with those of phospho-olivine LFP indexed with orthorhombic Pnma space group. The diffraction peaks of the n-LFP@C and c-LFP@C become much sharper, suggesting improved crystallinity of LFP. According to the nitrogen adsorption/desorption isotherms (Fig. S2), the Brunauer-Emmett-Teller surface areas of the n-LFP@C and c-LFP@C are 10.7 and 38.0 m^2 g^{-1} (Table S1), respectively. The X-ray photoelectron spectroscopy (XPS) spectra (Figs. S3a and S3b) further demonstrate that the Fe 2p spectra of LFP@C composite are split into two parts as a result of spin–orbit coupling and each part consists of a main peak and its satellite or shoulder peak, which is characteristic for Fe^{2+}.[25]

Figure 3 gives the HRTEM images of carbon-coated LFP particles (sample n-LFP@C and c-LFP@C). The slices with a thickness of 15 nm of the c-LFP@C in Figure 3d and the n-LFP@C particles with a thickness of 113 nm in Figure 3a. These results show that liquid crystal directing method can reduce the slice thickness observably. The lattice interplanar spacings of 0.34 nm is corresponding to the (111) plane and the thickness of the carbon layer is about 1.5 nm of n-LFP@C (Fig. 3b), respectively. However, Figure 3e shows that the carbon layer coated on the c-LFP@C is about 1.5 nm thick. As we know, the role of carbon is to improve the electric conductive of LFP and this electron transform process take place on the interface between LFP and carbon. Therefore, the synthesized LFP/C with same thickness of carbon layer is the key we had focused. As Figures 3b and 3e showed, the thickness of carbon layer on the c-LFP@C and n-LFP@C are almost the same.

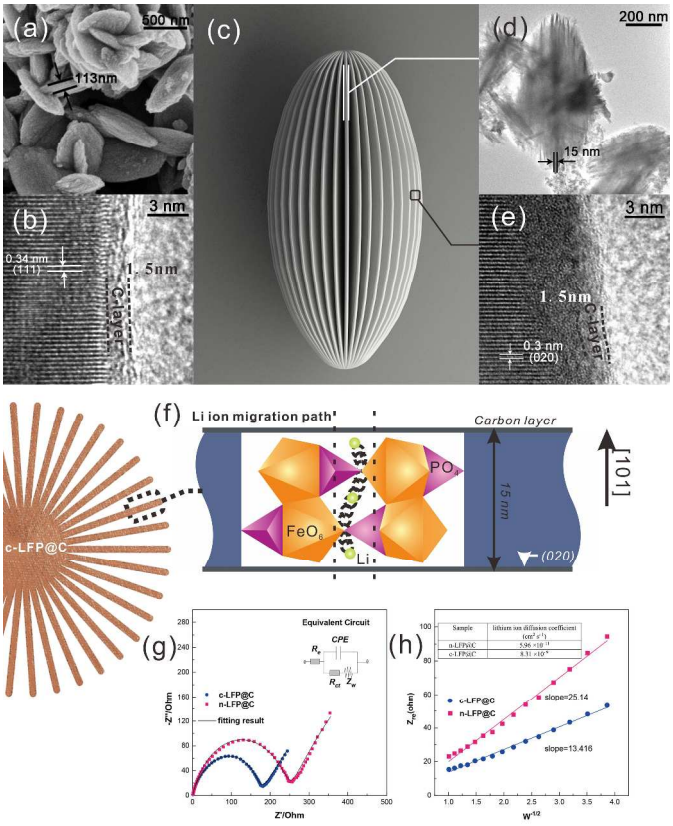

Figure 3. (a) SEM and (b) HRTEM of n-LFP@C. (c) Schematic illustration, (d) TEM and (e) HRTEM images of c-LFP@C. (f) Curved trajectories for Li ion migration between sites in the [010] direction. (g) EIS spectra of n-LFP@C and c-LFP@C and (h) Z' vs. ω−0.5 plots in the low-frequency region obtained.

Figure 3e also shows clear crystal lattices which lattice interplanar spacings of 0.3 nm is corresponding to the (020) plane. This result demonstrates that the Li^+ migration path in olivine $LiFePO_4$ is along the $[010]_{Pnma}$ direction. And the thickness of LFP layer determined the length of Li^+ migration channel. Therefore, the reduced of slice thickness (15 nm showed in Fig. 3(d)) can decline the overpotential and capacity fading resulting from volume changes and allow better reaction kinetics at the electrode surface, reflect in improved rate performances. Figure 3c shows the schematic illustration of c-LFP@C.

It is often assumed that the migrating ion takes the shortest path between adjacent sites, that is, a direct linear jump. However, the favored migration mechanism (migration between adjacent Li ion sites along the [010] direction) along the [010] channel reveals a small deviation from the linear (straight) route involving a curved path between adjacent Li sites. This produces a "wavelike" trajectory for long-range migration as illustrated in Figure 3f [22] and results in a lower migration energy than if the Li ion followed a direct, linear path. In addition, the carambola-like structure enhance the Li ion migration efficiency tremendously, resulting from the interface area of about 38.0 m^2 g^{-1} (Table S1).

Electrochemical impedance spectroscopy (EIS) examination was conducted to further clarify the difference in the electrochemical response of two carbon coated LFP cathode materials. As depicted in Figure 3g, these impedance spectra combined of a depressed semicircle in the high frequency region and a straight line in the low-frequency region, and a simple equivalent circuit was established to simulate the spectra (the inset in Fig. 3g). The semicircle is mainly associated to the charge-transfer resistance and the corresponding capacitance at the electrode/electrolyte interface, the straight line in the low frequency region is related with the diffusion behavior of lithium ions.[26-28] The charge-transfer resistance (R_{ct}) is calculated from the semicircle in the high-middle frequency range as about 180 Ω and 255 Ω for the c-LFP@C and n-LFP@C (Table inset in Fig. 3h), respectively, c-LFP@C electrode exhibits lower charge-transfer resistance, suggesting that their electrolyte-electrode complex reactions can occur easily. The smaller slope of impedance of n-LFP@C samples indicates their higher electrochemical activity, which ascribed to hierarchical porous structure facilitate the diffusion path of lithium ion. The improved lithium-ion diffusion process within c-LFP@C particles estimated from the oblique line at low frequencies is greatly enhanced by uniform carbon coating and electrolyte penetration, improving the electronic conductivity and reducing the diffusion path of the lithium ions.

$$Z_{Re} = R_e + R_{ct} + \sigma_w \omega^{-1/2} \quad (1)$$

$$D = \frac{R^2T^2}{2A^2n^4F^4C^2\sigma^2} \quad (2)$$

Figure 3h shows the relationship between Z_{Re} and square root of frequency ($\omega^{-1/2}$) in the low frequency region. With Equation 1, it is obtained that the Warburg impedance coefficient (σ_w) of the LFP samples, which are 13.416 and 25.14 cm^2 $s^{-1/2}$, respectively for c-LFP@C and n-LFP@C. Based on the obtained Warburg impedance coefficients, the Li ion diffusion coefficients of samples can be calculated using Equation 2,[29, 30] the Li ion diffusion coefficients of the n-LFP@C and c-LFP@C are extracted to be 5.96 $\times 10^{-11}$ and 8.31 $\times 10^{-9}$ cm^2 s^{-1}, respectively. The results clearly manifest that the Li ion diffusion coefficient of LFP nanocomposites could be increased with the decrease of Li ion migration path which would improve the conductive interconnection among the adjacent LFP particles. And enhanced with further load of the carbon layer which forms more conductive paths for electrons improve the electrons transfer efficiency and benefit the electrical conductivity of LFP. This clearly indicates that the liquid crystal directing method reduces the resistance, enhancing the charge transfer across the electrode-electrolyte interface.

Figures 4a and 4b display the galvanostatic charge and discharge voltage profiles of cells for LFP@C samples at progressively increasing C rates from 0.1 to 20 C between 2.5 and 4.2 V vs. Li^+/Li. Figure S4 compares the cyclic voltammetry (CV) curves of c-LFP@C and n-LFP@C samples at a scanning rate of 0.1 mV s^{-1} in the potential window of 2.5 to 4.2 V vs. Li^+/Li. All the CV curves exhibit only one pair of well-defined anodic and cathodic peaks, which represent the Li^+ deintercalation and reintercalation processes in the $LiFePO_4$ crystal lattice, respectively. Accordingly, the dependence of specific capacity on current density is shown in Figure 4c. The c-LFP@C materials exhibit higher capacities than n-LFP@C at a low rate 0.1 C, and a maximum capacity of 167.3 mA h g^{-1} (nearly to its theoretical capacity 170 mA h g^{-1}), while that of the n-LFP@C reachs 148.8 mA h g^{-1}. n-LFP@C displays lower capacity than c-LFP@C because of the lower lithium diffusion constant and electronic conductivity. Meanwhile, the result presents a serious polarization tendency at high C rates, while the c-LFP@C has a slight polarization tendency. It is noted the voltage plateau is lengthened for the cholesteryl benzoate c-LFP@C materials, which should be attributed to the higher electrochemical reactivity of c-LFP@C and excellent kinetics. Figure 4d shows the rate capabilities of LFP@C samples. When the C-rate increases from 0.1 to 20 C, c-LFP@C shows more satisfactory rate capability compared with n-LFP@C. It can be inferred that the structure with prior crystal growth on (020) plane plays a significant role in improving the reaction kinetics of LFP, especially at high discharge rates (it could also remain 50% of theory capacity at 20 C), and this is also consistent with EIS measurements (Figs 3g and 3h). We believe that the superior Li ion migration rate and electrical conductivity of c-LFP@C lead to the enhanced rate performance.

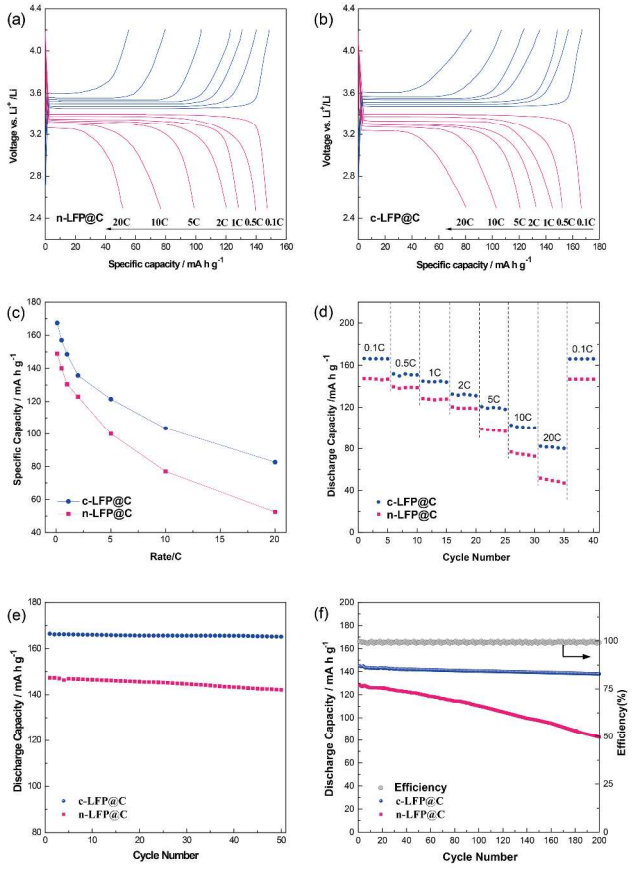

Figure 4. Initial voltage vs. capacity curves of (a) n-LFP@C and (b) c-LFP@C. (c) The dependence of specific capacity on current density rate capabilities and (d) rate capabilities of n-LFP@C and c-LFP@C. Cycling performance at (e) 0.1C and (f) 1C of sample n-LFP@C and c-LFP@C.

Figures 4e and 4f show the cycling performance of sample n-LFP@C and c-LFP@C particles at 0.1 and 1 C. Figure 4e shows the cyclability of c-LFP@C and n-LFP@C cathode at the low current

rate of 0.1 C. After 50 cycle, the cells still delivered a capacity of 165.7 (c-LFP@C, average 99.5% capacity retention) and 145.7 mA h g^{-1} (n-LFP@C, average 98.8% capacity retention), demonstrating ultra-high cyclability at low current rate for the c-LFP@C nanocomposites. Another excellent property of the c-LFP@C is the superior cycling performance. The discharge capacity of c-LFP@C is correspond to 138.1 mA h g^{-1} over 200 cycles at a rate of 1 C. And the Coulombic efficiency (calculated from the discharge capacity/charge capacity) always approaches 100%, as shown in the inset of Figure 4f.

Conclusions

In summary, we have developed a new method using cholesteric benzoate as structure-directing agent to synthesis LFP. A carambola-like LFP is prepared, which consists of LFP thin layers with significantly shortened [010] channel of ~15 nm with selectively exposed (020) plane. The unique structure greatly promotes the Li^+ diffusion along the preferential direction for Li storage, bringing an unprecedented Li^+ diffusion coefficient of 8.31×10^{-9} cm^2 s^{-1}. On the other hand, we have successfully coated a highly-conductive unltrathin carbon layer with controllable thickness (~1.5 nm) onto the surface of $LiFePO_4$ sheets, enabling fast electron transportation along the two-dimensional sheet. With the structural advantages of both components, a hierarchically mixed conducting network is formed, and the composite exhibits stable and extremely fast kinetics upon Li storage, which promises its use for high-power batteries with long lifespan. The composite exhibits stable and extremely fast electrochemistry upon Li storage by delivering almost a theoretical capacity (167 mA h g^{-1}) at 0.1 C and ~50% of the theoretical capacity (82 mA h g^{-1}) at a high rate of 20 C, and exhibits stable cycling performances at different rates. In view of its favorable electrochemical performances, the composite material may find its use in LIBs with stable cyclability and high energy output for emerging EV applications. The strategy is simple, yet effective, and can bring inspirations to those working on high-energy batteries. All these will contribute to a better economic sustainability to benefit the whole industry.

Notes and references

[a] School of Chemistry and Chemical Engineering, Hefei University of Technology, Hefei 230009, PR China.
[b] Department of Chemistry, University of Science and Technology of China, Hefei 230026, PR China.
* Prof. Dr. Xueliang Li, E-mail: xueliangli2005@163.com
†Electronic Supplementary Information (ESI) available: [details of any supplementary information available should be included here]. See DOI: 10.1039/c000000x/

1. B. Kang and G. Ceder, *Nature*, 2009, **458**, 190-193.
2. M. Contestabile, G. Offer, R. Slade, F. Jaeger and M. Thoennes, *Energy Environ. Sci.*, 2011, **4**, 3754-3772.
3. O. K. Park, Y. Cho, S. Lee, H.-C. Yoo, H.-K. Song and J. Cho, *Energy Environ. Sci.*, 2011, **4**, 1621-1633.
4. L. Ji, M. Rao, H. Zheng, L. Zhang, Y. Li, W. Duan, J. Guo, E. J. Cairns and Y. Zhang, *J. Am. Chem. Soc.*, 2011, **133**, 18522-18525.
5. A. K. Padhi, K. Nanjundaswamy and J. B. d. Goodenough, *J. Electrochem. Soc.*, 1997, **144**, 1188-1194.
6. A. Padhi, K. Nanjundaswamy, C. Masquelier, S. Okada and J. Goodenough, *J. Electrochem. Soc.*, 1997, **144**, 1609-1613.
7. L.-X. Yuan, Z.-H. Wang, W.-X. Zhang, X.-L. Hu, J.-T. Chen, Y.-H. Huang and J. B. Goodenough, *Energy Environ. Sci.*, 2011, **4**, 269-284.
8. L. Wang, X. He, W. Sun, J. Wang, Y. Li and S. Fan, *Nano Lett.*, 2012, **12**, 5632-5636.
9. Y. Wu, Z. Wen and J. Li, *Adv. Mater.*, 2011, **23**, 1126-1129.
10. C. Zhang, X. He, Q. Kong, H. Li, H. Hu, H. Wang, L. Gu, L. Wang, G. Cui and L. Chen, *CrystEngComm*, 2012, **14**, 4344-4349.
11. X. Lou and Y. Zhang, *J. Mater. Chem.*, 2011, **21**, 4156-4160.
12. L. Shen, C. Yuan, H. Luo, X. Zhang, K. Xu and Y. Xia, *J. Mater. Chem.*, 2010, **20**, 6998-7004.
13. L. Gu, C. Zhu, H. Li, Y. Yu, C. Li, S. Tsukimoto, J. Maier and Y. Ikuhara, *J. Am. Chem. Soc.*, 2011, **133**, 4661-4663.
14. K. Weichert, W. Sigle, P. A. van Aken, J. Jamnik, C. Zhu, R. Amin, T. Acartuerk, U. Starke and J. Maier, *J. Am. Chem. Soc.*, 2012, **134**, 2988-2992.
15. X. L. Wu, Y. G. Guo, J. Su, J. W. Xiong, Y. L. Zhang and L. J. Wan, *Adv. Energy Mater.*, 2013, **3**, 1155-1160.
16. Y. Wang, Y. Wang, E. Hosono, K. Wang and H. Zhou, *Angew. Chem. Int. Ed.*, 2008, **47**, 7461-7465.
17. S. W. Oh, S. T. Myung, S. M. Oh, K. H. Oh, K. Amine, B. Scrosati and Y. K. Sun, *Adv. Mater.*, 2010, **22**, 4842-4845.
18. C. Sun, S. Rajasekhara, J. B. Goodenough and F. Zhou, *J. Am. Chem. Soc.*, 2011, **133**, 2132-2135.
19. H. L. Fei, Z. W. Peng, Y. Yang, L. Li, A. R. O. Raji, E. L. G. Samuel and J. M. Tour, *Chem Commun.*, 2014, **50**, 7117-7119.
20. J. Yang, J. Wang, X. Li, D. Wang, J. Liu, G. Liang, M. Gauthier, Y. Li, D. Geng, R. Li and X. Sun, *J. Mater. Chem.*, 2012, **22**, 7537-7543.
21. A. Vu and A. Stein, *Chem. Mater.*, 2011, **23**, 3237-3245.
22. M. S. Islam, D. J. Driscoll, C. A. Fisher and P. R. Slater, *Chem. Mater.*, 2005, **17**, 5085-5092.
23. H. Takezoe and Y. Takanishi, Jpn. *J. Appl. Phys.* 2006, **45**, 597-625.
24. P. De Gennes and J. Prost, Oxford University Press, New York, Olbrich E., Marinov O., Davidov D., *Phys. Rev. E*, 1993, 2713, **48**.
25. M. Bhuvaneswari, N. N. Bramnik, D. Ensling, H. Ehrenberg and W. Jaegermann, *J. Power Sources*, 2008, **180**, 553-560.
26. T. Muraliganth, A. V. Murugan and A. Manthiram, *J. Mater. Chem.*, 2008, **18**, 5661-5668.
27. J. Xiang, J. Tu, L. Zhang, X. Wang, Y. Zhou, Y. Qiao and Y. Lu, *J. Power Sources*, 2010, **195**, 8331-8335.
28. X. L. Li, W. Guo, Y. F. Liu, W. X. He and Z. H. Xiao, *Electrochim. Acta*, 2014, **116**, 278-283.
29. J. Chlistunoff, D. Cliffel and A. J. Bard, *Thin Solid Films*, 1995, **257**, 166-184.
30. A. Bard and L. Faulkner, *Electrochemical methods*; Wiley: New York, 1980.

